Estimating the Ionospheric Induction Electric Field using Ground Magnetometers

Michael Madelaire[1], Karl Laundal[1], Spencer Hatch[1], Heikki Vanhamäki[2], Jone Reistad[1], Anders Ohma[1], Viacheslav Merkin[4], Dong Lin[3]

[1]Department of Physics and Technology, University of Bergen, Bergen, Norway
[2]Space Physics and Astronomy Research Unit, University of Oulu, Oulu, Finland
[3]High Altitude Observatory, National Center for Atmospheric Research, Boulder, CO, USA
[4]Applied Physics Laboratory, Johns Hopkins University, Laural, MD, USA

Key Points:

- A method for estimating the induction electric field using ground magnetometer measurements is presented.
- Locally, the induction electric field can constitute tens of percent of the total electric field, during the sudden commencement examined.
- The spatial pattern of ionospheric Joule heating is shown to be highly affected by the induction electric field, even during weak induction.

Corresponding author: Michael Madelaire, michael.madelaire@uib.no

Abstract

The ionospheric convection electric field is often assumed to be a potential field. This assumption is not always valid, especially when the ionosphere changes on short time scales $T \lesssim 5$ min. We present a technique for estimating the induction electric field using ground magnetometer measurements. The technique is demonstrated on real and simulated data for sudden increases in solar wind dynamic pressure of ∼1 and 10 nPa, respectively. For the real data, the ionospheric induction electric field is 0.15±0.015 mV/m, and the corresponding compressional flow is 2.5±0.3 m/s. For the simulated data, the induction electric field and compressional flow reach 3 mV/m and 50 m/s, respectively. The induction electric field can locally constitute tens of percent of the total electric field. Inclusion of the induction electric field increased the total Joule heating by 2.4%. Locally the Joule heating changed by tens of percent. This corresponds to energy dissipation that is not accounted for in existing models.

Plain Language Summary

In the study of ionospheric dynamics, it is often assumed that the ionospheric electric field is a potential field. This means the contribution from induction is neglected. The induction electric field is described by Faraday's law and relates to temporal changes in the magnetic field. This assumption only holds when the ionospheric dynamics change slowly. In this study, we present a technique for calculating the ionospheric induction electric field using measurements of the magnetic field on the ground. We demonstrate the technique on real and simulated data of a dynamic event, i.e. a sudden commencement. We find that the induction electric field, on a global scale, is small compared to the potential electric field. However, locally it can be relatively large. Similarly, the inclusion of the induction electric field increased the total energy dissipation, i.e. Joule heating, by only a couple of percent but resulted in local variations of tens of percent. Furthermore, we quantified and visualized the compression flow which is the compression and expansion of the magnetic field related to the temporal evolution of a dynamic ionospheric event.

1 Introduction

In this paper, we investigate the ionospheric induction electric field ($\boldsymbol{E}_{ind}$) using a new technique based on ground magnetometers. When studying ionospheric dynamics the ionospheric electric field ($\boldsymbol{E}$) is often assumed to be a potential field ($\boldsymbol{E}_{pot}$). This assumption can be very useful as it may simplify modeling efforts significantly. Techniques such as AMIE/AMGeO [Richmond and Kamide 1988]; [AMGeO Collaboration 2019] and Lompe [Laundal et al. 2022]; [Hovland et al. 2022] model $\boldsymbol{E}_{pot}$ by ignoring $\boldsymbol{E}_{ind}$ that otherwise is implied by Faraday's induction law ($\nabla \times \boldsymbol{E} = -\frac{\partial}{\partial t}\boldsymbol{B}$) [Faraday 1832]. Similarly, $\boldsymbol{E}_{ind}$ is almost always ignored in the ionospheric solvers used to account for the magnetosphere-ionosphere (MI) coupling in magnetohydrodynamic (MHD) simulations (e.g. Tanaka 2000; J. Lyon et al. 2004; Merkin and J. G. Lyon 2010. We present a technique for estimating $\boldsymbol{E}_{ind}$ based on measurements of ground magnetic perturbation. Essentially, allowing $\boldsymbol{E}_{ind}$ to be measured from ground.

Transient events (e.g. sudden commencements or substorm expansions) can result in large changes in the magnetic field ($\boldsymbol{B}$) on a timescale of seconds or minutes. When ignoring Faraday's law the mutual interaction between the electrostatic and inductive processes is neglected which can be important during dynamic events. Yoshikawa and Itonaga 2000 provide a detailed explanation of the inductive ionosphere, from an $\boldsymbol{E}$,$\boldsymbol{J}$ perspective [Vasyliūnas 2012]. It is well known that field-aligned currents (FACs) close through the ionosphere via a divergent Pedersen current, assuming the ionospheric conductance is uniform and the system is in steady state. When a magnetospheric driver is changed, e.g. the opening of a magnetic field line and subsequent anti-sunward con-

vection, the information is communicated via shear Alfvén waves. Bending a magnetic field line, in the conductive ionosphere, excites a flow of electrons perpendicular to the direction of the bend (i.e. Ampere's law) which constitutes a rotational electric field, i.e. $\boldsymbol{E}_{ind}$. Again, assuming uniform conductance, the flow of electrons is a divergent Hall current. Because the electrons are *frozen-in* they act to compress/expand magnetic flux, i.e. $\frac{\partial}{\partial t}\boldsymbol{B}$. We refer to this as *compression flow* ($\boldsymbol{E}_{ind}\times\boldsymbol{B}$). The compression flow is necessary to alter the distribution of magnetic flux to facilitate the ionospheric closure current carried by ions and a new steady state. In other words, in steady state and uniform conductance, the Pedersen current closing FACs only exist due to a pre-existing divergent Hall current. The rate of change in the ionosphere depends on the Pedersen conductance (Σ_P). Southwood and Kivelson 1991 derived a decay rate ($\gamma \propto \Sigma_P^{-1}$) describing the time it takes for the ionospheric current system to change. Additionally, Dreher 1997 simulated the MI coupling with inductive terms and showed that the time it takes a FAC to reach steady state varies with Σ_P.

Vanhamäki et al. 2005 investigated the inductive effect on the ionospheric electric field using realistic time-dependent three-dimensional models of the high latitude ionospheric current system. They found that ionospheric self-induction is locally important with $\boldsymbol{E}_{ind}$ reaching a few mV/m. Vanhamäki et al. 2006 presented a new technique for calculating $\boldsymbol{E}_{ind}$ in a non-uniform conducting ionosphere. The technique utilizes the Cartesian elementary current system technique and requires $\boldsymbol{E}_{pot}$ and Hall/Pedersen conductances as input. Vanhamäki et al. 2007 applied this technique to derive $\boldsymbol{E}_{ind}$ for a westward traveling surge, Ω-band, and intensifying electrojet. They found that $\boldsymbol{E}_{ind}$ can reach magnitudes of several tens of percent of the total electric field. Takeda 2008 simulated $\boldsymbol{E}_{ind}$ associated with FACs with periods of 60, 10, 4, and 1 min and found that $\boldsymbol{E}_{ind}$ had a non-negligible impact when the period of the FACs was 4 min or less.

In this study, we present a technique for estimating the ionospheric induction electric field based on ground magnetometer measurements represented with a spherical harmonic expansion and present examples of the associated ionospheric plasma flow. The purpose of the presented technique is to go beyond the assumption of a potential electric field in empirical modeling (e.g., AMIE and Lompe). Co-estimation of the potential and induction electric fields is desirable to understand the temporal evolution of the system. From a practical point of view, it also avoids the mapping of the induction electric field into the potential electric field. Additionally, by including the time-dependency of the system, the result becomes more constrained as subsequent time-steps are linked via measurements, increasing the overall information. However, the incorporation of this technique into pre-existing empirical modeling frameworks is outside the scope of the current study and will be addressed in future studies.

Our technique uses spatiotemporal variations in the magnetic field to infer compressional flow is analogous with studies of core flow using time-dependent models of Earth's main magnetic field (e.g. Finlay et al. 2020; Sabaka et al. 2020; Finlay et al. 2023). Spherical harmonic models of Earth's core magnetic field can provide information about changes in the motion of liquid metal in the outer core through estimates of secular variation. This information can be used as boundary conditions in models of Earth's dynamo [Schaeffer et al. 2016]. To the knowledge of the authors, it is the first time ground magnetometer measurements have been used to inform about the inductive component of the ionospheric electric field. However, Vanhamäki et al. 2013 solved Faraday's law based on the radial magnetic field to derive the induced electric field at Earth's surface.

In Section 2 we present a technique for deriving the ionospheric $\boldsymbol{E}_{ind}$ from ground magnetic field perturbations. A more thorough derivation is provided in the Supporting Information. In Section 3, the technique is demonstrated using synthetic data from a coupled geospace model presented by Shi et al. 2022 and real ground magnetometer measurements during sudden commencements (SCs). Section 4 discusses the results.

2 Technique

In this section, we describe how an estimate of the ionospheric induction electric field ($\boldsymbol{E}_{ind}$) can be derived from the temporal derivative of the radial magnetic field $\left(\frac{\partial}{\partial t}B_r\right)$ below the ionosphere. A more in-depth derivation is provided in the Supporting Information.

The ionospheric electric field ($\boldsymbol{E}$) can be decomposed into three scalar fields using the *alternative Helmholtz representation* [Sabaka et al. 2010],

$$\boldsymbol{E} = U\hat{\boldsymbol{r}} + \boldsymbol{\nabla}_S V - \hat{\boldsymbol{r}} \times \boldsymbol{\nabla}_S W. \tag{1}$$

Here $\hat{\boldsymbol{r}}$ is the radial unit vector and $\boldsymbol{\nabla}_S$ is the angular portion of the $\boldsymbol{\nabla}$ operator.

The curl of the ionospheric electric field ($\boldsymbol{\nabla} \times \boldsymbol{E}$) on a spherical shell can be described by $\frac{\partial}{\partial t}B_r$ on the shell according to Faraday's law. By inserting Equation 1 into Faraday's law $\frac{\partial}{\partial t}B_r$ can be expressed in terms of W,

$$\frac{\partial}{\partial t}B_r = \hat{\boldsymbol{r}}\boldsymbol{\nabla}^2 W. \tag{2}$$

The scalar field W can be represented with a Spherical Harmonic (SH) expansion,

$$W = \sum_{n=1}^{N}\sum_{m=0}^{n}\left[a_n^{m,W}\cos(m\phi) + b_n^{m,W}\sin(m\phi)\right]P_n^m\left(\cos(\theta)\right). \tag{3}$$

Here (θ, ϕ) are colatitude and longitude, (n, m) are the SH degree and order, ($a_n^{m,W}$, $b_n^{m,W}$) are the SH coefficients, and $P_n^m\left(\cos(\theta)\right)$ is the Schmidt quasi normalized Legendre polynomial. The coefficients ($a_n^{m,W}$, $b_n^{m,W}$) are unknown, but can be expressed in terms of the SH coefficients ($\frac{\partial}{\partial t}a_n^{m,B}$, $\frac{\partial}{\partial t}b_n^{m,B}$) related to a SH expansion of $\frac{\partial}{\partial t}B_r$ following Sabaka et al. 2010,

$$\begin{aligned} a_n^{m,W} &= \frac{r^2}{n+1}\frac{\partial}{\partial t}a_n^{m,B} \\ b_n^{m,W} &= \frac{r^2}{n+1}\frac{\partial}{\partial t}b_n^{m,B}. \end{aligned} \tag{4}$$

In practice $a_n^{m,B}$ and $b_n^{m,B}$ can be determined by solving a linear inverse problem with magnetic field measurements on ground as input. The resulting SH coefficients should be determined using the ionosphere as their reference height. However, if the coefficients are determined with Earth's surface as their reference height they can simply be upward continued to the ionosphere. This detail is important as it defines the altitude of the spherical shell on which $\boldsymbol{E}_{ind}$ will be determined. Only the radial magnetic field component can be upward continued to the ionosphere because it is continuous across boundary layers, unlike the horizontal components.

The horizontal part of $\boldsymbol{E}_{ind}$ is given by the last term of Equation 1,

$$\boldsymbol{E}_{ind,h} = -\hat{\boldsymbol{r}} \times \boldsymbol{\nabla}_S W = -\hat{\boldsymbol{r}} \times \boldsymbol{\nabla} W. \tag{5}$$

In the ionosphere, where the field-aligned conductivity is high, the electric field maps along the magnetic field making $\boldsymbol{E}\cdot\boldsymbol{B} = 0$. This allows for the determination of $E_{ind,r}$. However, $\boldsymbol{E}_{pot}$ is typically unknown. By assuming radial magnetic field lines $E_{ind,r} = -E_{pot,r}$ and the compression flow is given as

$$\boldsymbol{v} = \frac{\boldsymbol{E}_{ind} \times \hat{\boldsymbol{b}}_r}{B}, \tag{6}$$

where $\hat{\boldsymbol{b}}_r = -\hat{\boldsymbol{r}}$ in the northern hemisphere.

Through the merger of the technique presented here and empirical modeling techniques of the ionospheric potential electric field like AMIE and Lompe $\boldsymbol{E}_{pot}$ and $\boldsymbol{E}_{ind}$ might be co-estimated. This will be the focus of future studies.

3 Results

Estimating the induction electric field ($\boldsymbol{E}_{ind}$) requires a SH model of $\frac{\partial}{\partial t}B_r$. In this section, we apply our method to two different cases of SCs. One model is based on ground magnetic perturbations from an MHD simulation while the other is based on real ground magnetometer measurements.

3.1 Synthetic data example

The synthetic data is based on an MHD simulation of an interplanetary shock carried out and analyzed by Shi et al. 2022. During this event, the solar wind dynamic pressure increases by approximately 10 nPa. The RE-developed Magnetosphere-Ionosphere Coupler/Solver (REMIX) [Merkin and J. G. Lyon 2010] is used to determine the ionospheric current and assumes that $\boldsymbol{\nabla}\times\boldsymbol{E} = 0$. The reader is referred to Shi et al. 2022 for further details regarding the simulation. The ground magnetic perturbation is determined by computing a Biot-Savart integral over the ionospheric currents, FACs, and magnetospheric currents on an equal area grid with a 0.5 degree latitudinal resolution down to 0° latitude. We represent the ground magnetic perturbation using SHs, where the SH coefficients ($a_n^{m,B}$, $b_n^{m,B}$) are determined by solving an inverse problem similar to Madelaire et al. 2022a with the SH expansion truncated at $n = 100$. The SH expansion is only done for external sources as the synthetic data does not include ground induction.

Figure 1 summarizes the technique for estimating $\boldsymbol{E}_{ind}$, using synthetic data of the preliminary impulse associated with a SC. Figure 1a shows $\frac{\partial}{\partial t}B_r$ on ground. Figure 1b shows a recreation of $\frac{\partial}{\partial t}B_r$ using a SH model based on ground magnetic perturbation. A comparison between Figures 1a-b shows that $\frac{\partial}{\partial t}B_r$ is reproduced well by the SH model. Figures 1c-d compare the estimated $\boldsymbol{E}_{ind}$ and the ionospheric potential electric field ($\boldsymbol{E}_{pot}$) from the MHD simulation. Comparison between $\boldsymbol{E}_{ind}$ and $\boldsymbol{E}_{pot}$ are done with respect to the first of the two subsequent timesteps used to determine $\frac{\partial}{\partial t}B_r$. We find that $\boldsymbol{E}_{ind}$ reaches up to 3 mV/m which locally can correspond to tens of percent of $\boldsymbol{E}$ ($\boldsymbol{E} = \boldsymbol{E}_{pot} + \boldsymbol{E}_{ind}$) in the high latitude ionosphere. Therefore, $\boldsymbol{E}_{ind}$ can have a significant regional impact. Figure 1e shows Joule heating associated with $\boldsymbol{E}_{pot}$ (i.e. $\Sigma_p E_{pot}^2$) which is a result of maintaining the steady state current system. Figure 1f shows the difference in Joule heating when including $\boldsymbol{E}_{ind}$, i.e. $\Sigma_P \left[E_{pot}^2 + 2(\boldsymbol{E}_{pot}\cdot\boldsymbol{E}_{ind}) + E_{ind}^2\right]$. The difference can locally be tens of percent, both positive and negative. However, the total Joule heating above 50 degrees latitude only increases by approximately 2.4%. The pins in Figures 1e-f illustrate the steady state convection and compression flow (Equation 6), respectively, where B is the magnitude of a dipole magnetic field. The dipole magnetic field is determined using the first SH degree of IGRF-12 [Thébault et al. 2015]. The flow illustrates the expansion/compression of magnetic flux necessary to change the ionospheric current system from one steady state to another.

3.2 Real data example

The SH model based on real ground magnetometer measurements was provided by Madelaire et al. 2022a and is the product of a superposed epoch analysis of SCs. Madelaire et al. 2022a presented 12 models determined by dividing the list of SCs presented by Madelaire et al. 2022b into 12 groups based on the Interplanetary Magnetic Field (IMF) clock angle and dipole tilt angle. In this example, we use the model created for SCs during northward IMF and positive dipole tilt (Summer in the northern hemisphere). The model is based on 175 events, the majority of which experience solar wind dynamic pressure increases around 1–2 nPa. The much smaller pressure increases in this model compared to that used in Section 3.1 results in significantly smaller $\frac{\partial}{\partial t}B_r$ and $\boldsymbol{E}_{ind}$. The SH model includes a separation between internal and external sources. Both sets of SH coefficients are upward continued to the ionosphere and combined before deriving $\boldsymbol{E}_{ind}$.

Furthermore, to assess uncertainty, 50 realizations of the model were created by resampling the events used as input.

Figure 2 shows a time series of $\frac{\partial}{\partial t}B_r$ and compression flow associated with the SH model, based on real ground magnetometer measurements, starting 2 minutes prior to the initial increase in SYM-H [Iyemori et al. 2010]. Epochs are synonymous with minutes. Here, $\frac{\partial}{\partial t}B_r$ is the median across all 50 model realizations and the compression flow is the bias vector (e.g. Haaland et al. 2007) scaled with the median magnitude. The preliminary impulse appears in Figures 2a-b. The main impulse appears in Figure 2c, equatorward and with the opposite polarity of the preliminary impulse. Over the following 3 minutes (i.e. Figures 2d-f) the main impulse expands along the flanks toward the nightside while increasing in strength. The compression flow is around 2.5 m/s with a standard deviation of around 0.3 m/s. Additionally, a large-scale southward flow appears shortly after the appearance of the preliminary impulse.

4 Discussion

We presented a technique for estimating the ionospheric induction electric field ($\boldsymbol{E}_{ind}$) using measurements of magnetic field perturbation below the ionosphere. The technique links a SH representation of the temporal derivative of the radial magnetic field ($\frac{\partial}{\partial t}B_r$) to a scalar field W representing $\boldsymbol{E}_{ind}$. In an example with synthetic data, we found that $\boldsymbol{E}_{ind}$ reaches values of 3 mV/m (Figure 1d) which locally can correspond to tens of percent of the combined ionospheric electric field ($\boldsymbol{E} = \boldsymbol{E}_{pot} + \boldsymbol{E}_{ind}$) in the high latitude ionosphere. From estimates of $\boldsymbol{E}_{ind}$ a compression flow of approximately 50 m/s was calculated (Figure 1b), which represents the necessary expansion/contraction of magnetic flux to reach a new steady state. The total Joule heating above 50 degrees latitude increased by approximately 2.4% while local changes were tens of percent (see Figures 1e-f). Inclusion of $\boldsymbol{E}_{ind}$ in the calculation of Joule heating adds two terms, i.e. $\Sigma_P E_{ind}^2$ and $2\Sigma_P(\boldsymbol{E}_{pot} \cdot \boldsymbol{E}_{ind})$. Assuming $E_{ind} = E_{pot}/10$ results in E_{ind}^2 being 1% of E_{pot}^2. Meanwhile, the cross-term can contribute up to 20% of the Joule heating depending on the alignment of $\boldsymbol{E}_{ind}$ and $\boldsymbol{E}_{pot}$. However, the cross-term can be positive or negative. It is, therefore, unclear how much it contributes to the total heating when integrated over the entire ionosphere. The contribution from the cross-term is illustrated in Figure 1f and leads to a significant difference in ionospheric energy dissipation during dynamic events compared to the steady state case, even when E_{ind} is an order of magnitude smaller than E_{pot}. However, the estimated value of 2.4% is specific for the synthetic case being studied as both the magnitude and spatial extent of the temporally varying magnetic field depend on several exogenous parameters. Furthermore, the background level of Joule heating can also vary.

The MHD simulation carried out by Shi et al. 2022, used to create the synthetic data example in Section 3.1, applied the ionospheric solver REMIX [Merkin and J. G. Lyon 2010] which assumes steady state. Therefore, the ionospheric electric field is a potential electric field since ionospheric self-inductance is neglected (i.e $\boldsymbol{\nabla}\times\boldsymbol{E} = \frac{\partial}{\partial t}\boldsymbol{B} = 0$). We calculate $\frac{\partial}{\partial t}\boldsymbol{B}$ as the difference between two steady states for demonstration purposes. The combined ionospheric electric field (i.e. $\boldsymbol{E} = \boldsymbol{E}_{pot} + \boldsymbol{E}_{ind}$) no longer satisfy the current continuity ($\boldsymbol{\nabla} \cdot \boldsymbol{J} = 0$) ensured in REMIX and is fundamentally inconsistent. Furthermore, the rotational current associated with $\boldsymbol{E}_{ind}$ in Figure 1d contributes to the ground magnetic perturbation. This leads to a secondary and weaker induction effect which subsequently leads to a third and so on and so forth. The infinite chain of opposing and progressively induction effects is naturally accounted for when using real data. However, the synthetic data still provide insight into the usefulness of the presented technique. The magnitude of $\boldsymbol{E}_{ind}$ is similar to previous studies [Vanhamäki et al. 2005]; [Vanhamäki et al. 2007].

The presented technique was also used on a SH model of SCs based on real ground magnetometer measurements [Madelaire et al. 2022a]. The retrieved $\boldsymbol{E}_{ind}$ and compression flow is around 0.15±0.015 mV/m and 2.5±0.3 m/s (Figure 2), respectively. Additionally, the compression flow is dominated by a large-scale southward flow. This is consistent with an intensification of the magnetic perturbation from magnetospheric sources due to compression of the magnetosphere. The same intensification gives rise to a step-like increase in SYM-H during SCs [Russell et al. 1994]; [Madelaire et al. 2022b]. A large-scale flow is likewise present in the example with synthetic data, i.e. Figure 1f. In Figure 3 the contribution from magnetospheric currents to $\boldsymbol{E}_{ind}$ (i.e. Figure 3b) and the associated Joule heating has been separated from that of ionospheric currents and FACs (i.e. Figure 3c) for the synthetic example. Magnetospheric currents (e.g. magnetopause and ring current) produce, to first order, a uniform magnetic field in $\hat{\boldsymbol{z}}$. At the poles, this corresponds to a weakening of the magnetic field, an azimuthal induction electric field (westward on the dayside), and a large-scale southward flow in the northern hemisphere. The induction electric field in the southern hemisphere points in the same direction but $\hat{\boldsymbol{b}}$ points outward giving rise to a large-scale northward compression flow. Essentially, there is a large-scale equatorward compression flow at high latitude in response to rapid increases in solar wind dynamic pressure. Oppositely, there is a large-scale poleward compression flow in response to rapid decreases in solar wind dynamic pressure.

It is unclear how to interpret local changes in Joule heating due to the inclusion of $\boldsymbol{E}_{ind}$. Hesse et al. 1997 showed that $\boldsymbol{E}$ maps between the ionosphere and magnetosphere for ideal MHD, i.e. including inductive terms. If that holds in reality it would lead to an asymmetric spatiotemporal evolution, e.g. during SCs. However, Hesse et al. 1997 also showed that the mapping is non-trivial in the presence of parallel electric fields. Regardless of how $\boldsymbol{E}_{ind}$ maps between ionosphere and magnetosphere the spatiotemporal evolution of dynamic events, e.g. transient current vortices associated with the preliminary and main impulse of a SC and rapid compression/expansion of the magnetosphere, lead to significant local changes in Joule heating. The duration of these local changes can result in ion upflow but are unlikely to cause neutral upwelling [Strangeway 2012]. Zou et al. 2017 observed lifting of the F region ionosphere, large and transient field-aligned ion upflow, and prompt but short-lived ion temperature increase in the transition between the preliminary and main impulse of a sudden commencement using PFISR measurements.

There are significant differences in the magnitude of $\boldsymbol{E}_{ind}$ and the compression flow (Equation 6) between the two models. The SH model provided by Madelaire et al. 2022a is a product of a superposed epoch analysis based on a list of solar wind dynamic pressure increases [Madelaire et al. 2022b]. The majority of the events in the list are not interplanetary shocks, and experience smaller pressure increases compared to what is often seen in case studies and MHD simulations (e.g. Moretto et al. 2000; Slinker et al. 1999; Fujita et al. 2003. Madelaire et al. 2022b showed that the events, on average, contain increases of a couple of nPa. The interplanetary shock simulated by Shi et al. 2022 increased by approximately 10 nPa. The vast difference in the size of the pressure increase along with the smoothing associated with superposing multiple events leads to a $\frac{\partial}{\partial t}B_r$ in the order of 10 nT/min (Figure 2) compared to the 10 nT/s (Figure 1) seen in the MHD simulation. This is likely the explanation for the smaller compression flow.

The presented technique can be extended to the Spherical Elementary Current System (SECS) technique [Amm and Viljanen 1999]. The Lompe technique [Laundal et al. 2022]; [Hovland et al. 2022] models $\boldsymbol{E}_{pot}$ using SECS by combining various measurements (e.g. conductance, convection, and ground/space magnetic field measurements), similar to AMIE/AMGeO [Richmond and Kamide 1988]; [AMGeO Collaboration 2019]. However, the use of SECS in Lompe makes it ideal for regional analysis. In the future, we hope to remove the necessity of assuming steady state when using Lompe by implementing a scheme to co-estimate $\boldsymbol{E}_{pot}$ and $\boldsymbol{E}_{ind}$ using a technique similar to the one shown

here. Looking ahead, preliminary work suggests that data from EISCAT 3D [Kero et al. 2019] will open possibilities for empirical modeling frameworks of 3D ionospheric currents. Such advancements will allow us to move beyond the limitations of an infinitely thin ionosphere model. We might, therefore, revisit our technique in the future in attempts to expand it into 3D.

Acknowledgments

This work was funded by the Research Council of Norway (RCN) under contract 223252/F50. KL. and JR were also funded by the RCN under contract 300844/F50. KL. and SH were also funded by the Trond Mohn Foundation. VM and DL were funded by NASA DRIVE Science Center under cooperative Agreement 80NSSC22M0163.

Data Availability Statement

The synthetic data used in this study is available at Zenodo via `https://doi.org/10.5281/zenodo.8116401` Madelaire 2023. The spherical harmonic model based on real ground magnetometer observations was provided by Madelaire et al. 2022a and is available at Zenedo via `https://zenodo.org/record/6243103` Madelaire 2022.

References

AMGeO Collaboration (Dec. 2019). "A Collaborative Data Science Platform for the Geospace Community: Assimilative Mapping of Geospace Observations (AMGeO) v1.0.0". In: *Zenodo.* DOI: 10.5281/zenodo.3564914. URL: https://doi.org/10.5281/zenodo.3564914.

Amm, O. and A. Viljanen (June 1999). "Ionospheric disturbance magnetic field continuation from the ground to the ionosphere using spherical elementary current systems". In: *Earth, Planets and Space* 51.6, pp. 431–440. DOI: 10.1186/BF03352247. URL: https://doi.org/10.1186/BF03352247.

Dreher, J. (1997). "On the self-consistent description of dynamic magnetosphere-ionosphere coupling phenomena with resolved ionosphere". In: *Journal of Geophysical Research: Space Physics* 102.A1, pp. 85–94. DOI: https://doi.org/10.1029/96JA02800. eprint: https://agupubs.onlinelibrary.wiley.com/doi/pdf/10.1029/96JA02800. URL: https://agupubs.onlinelibrary.wiley.com/doi/abs/10.1029/96JA02800.

Faraday, M. (1832). "V. Experimental researches in electricity". In: *Philosophical Transactions of the Royal Society of London* 122, pp. 125–162. DOI: 10.1098/rstl.1832.0006. eprint: https://royalsocietypublishing.org/doi/pdf/10.1098/rstl.1832.0006. URL: https://royalsocietypublishing.org/doi/abs/10.1098/rstl.1832.0006.

Finlay, C. C., N. Gillet, J. Aubert, P. W. Livermore, and D. Jault (June 2023). "Gyres, jets and waves in the Earth's core". In: *Nature Reviews Earth & Environment* 4.6, pp. 377–392. DOI: 10.1038/s43017-023-00425-w. URL: https://doi.org/10.1038/s43017-023-00425-w.

Finlay, C. C., C. Kloss, N. Olsen, M. D. Hammer, L. Tøffner-Clausen, A. Grayver, and A. Kuvshinov (2020). "The CHAOS-7 geomagnetic field model and observed changes in the South Atlantic Anomaly". In: *Earth Planets Space* 72.156. DOI: https://doi.org/10.1186/s40623-020-01252-9.

Fujita, S., T. Tanaka, T. Kikuchi, K. Fujimoto, K. Hosokawa, and M. Itonaga (2003). "A numerical simulation of the geomagnetic sudden commencement: 1. Generation of the field-aligned current associated with the preliminary impulse". In: *Journal of Geophysical Research: Space Physics* 108.A12. DOI: https://doi.org/10.1029/2002JA009407.

Haaland, S. E., G. Paschmann, M. Förster, J. M. Quinn, R. B. Torbert, C. E. McIlwain, H. Vaith, P. A. Puhl-Quinn, and C. A. Kletzing (2007). "High-latitude plasma convection from Cluster EDI measurements: method and IMF-dependence". In: *Annales Geophysicae* 25.1, pp. 239–253. DOI: 10.5194/angeo-25-239-2007. URL: https://angeo.copernicus.org/articles/25/239/2007/.

Hesse, Michael, Joachim Birn, and Robert A. Hoffman (1997). "On the mapping of ionospheric convection into the magnetosphere". In: *Journal of Geophysical Research: Space Physics* 102.A5, pp. 9543–9551. DOI: https://doi.org/10.1029/96JA03999. eprint: https://agupubs.onlinelibrary.wiley.com/doi/pdf/10.1029/96JA03999. URL: https://agupubs.onlinelibrary.wiley.com/doi/abs/10.1029/96JA03999.

Hovland, A. Ø., K. M. Laundal, J. P. Reistad, S. M. Hatch, S. J. Walker, M. Madelaire, and A. Ohma (2022). "The Lompe code: A Python toolbox for ionospheric data analysis". In: *Frontiers in Astronomy and Space Sciences* 9. DOI: 10.3389/fspas.2022.1025823. URL: https://www.frontiersin.org/articles/10.3389/fspas.2022.1025823.

Iyemori, T., M. Takeda, M. Nose, and H. Toh (2010). "Mid-latitude Geomagnetic Indices ASY and SYM for 2009 (Provisional)". In: *Internal Report of Data Analysis Center for Geomagnetism and Space Magnetism, Kyoto University, Japan.*

Kero, J., D. Kastinen, J. Vierinen, T. Grydeland, C. Heinselman, J. Markkanen, and A. Tjulin (2019). "EISCAT 3D: the next generation international atmosphere and geospace research radar". In: *Proceedings of the First NEO and Debris Detection Conference.*

Laundal, K. M., J. P. Reistad, S. M. Hatch, M. Madelaire, S. Walker, A. Hovland, A. Ohma, V. Merkin, and K. Sorathia (May 2022). "Local Mapping of Polar Ionospheric Electrodynamics". In: *Journal of Geophysical Research: Space Physics* 127. DOI: 10.1029/2022JA030356.

Lyon, J.G., J.A. Fedder, and C.M. Mobarry (2004). "The Lyon–Fedder–Mobarry (LFM) global MHD magnetospheric simulation code". In: *Journal of Atmospheric and Solar-Terrestrial Physics* 66.15. Towards an Integrated Model of the Space Weather System, pp. 1333–1350. DOI: https://doi.org/10.1016/j.jastp.2004.03.020. URL: https://www.sciencedirect.com/science/article/pii/S1364682604001439.

Madelaire, M. (Feb. 2022). *List of rapid solar wind dynamic pressure increases.* Zenodo [Dataset]. DOI: 10.5281/zenodo.6243103. URL: https://doi.org/10.5281/zenodo.6243103.

— (May 2023). *Synthetic data for estimation of the ionospheric induction electric field.* Zenodo. [Dataset]. DOI: 10.5281/zenodo.8116401. URL: https://doi.org/10.5281/zenodo.8116401.

Madelaire, M., K. M. Laundal, J. P. Reistad, S. M. Hatch, and A. Ohma (2022a). "Transient high latitude geomagnetic response to rapid increases in solar wind dynamic pressure". In: *Frontiers in Astronomy and Space Sciences* 9. DOI: 10.3389/fspas.2022.953954. URL: https://www.frontiersin.org/articles/10.3389/fspas.2022.953954.

Madelaire, M., K. M. Laundal, J. P. Reistad, S. M. Hatch, A. Ohma, and S. Haaland (2022b). "Geomagnetic Response to Rapid Increases in Solar Wind Dynamic Pressure: Event Detection and Large Scale Response". In: *Frontiers in Astronomy and Space Sciences* 9. DOI: 10.3389/fspas.2022.904620. URL: https://www.frontiersin.org/article/10.3389/fspas.2022.904620.

Merkin, V. G. and J. G. Lyon (2010). "Effects of the low-latitude ionospheric boundary condition on the global magnetosphere". In: *Journal of Geophysical Research: Space Physics* 115.A10. DOI: https://doi.org/10.1029/2010JA015461. eprint: https://agupubs.onlinelibrary.wiley.com/doi/pdf/10.1029/2010JA015461. URL: https://agupubs.onlinelibrary.wiley.com/doi/abs/10.1029/2010JA015461.

Moretto, T., A. J. Ridley, M. J. Engebretson, and O. Rasmussen (2000). "High-latitude ionospheric response to a sudden impulse event during northward IMF conditions". In: *Journal of Geophysical Research: Space Physics* 105.A2, pp. 2521–2531. DOI: https://doi.org/10.1029/1999JA900475.

Richmond, A. D. and Y. Kamide (1988). "Mapping electrodynamic features of the high-latitude ionosphere from localized observations: Technique". In: *Journal of Geophysical Research* 93.A6, pp. 5741–5759. DOI: 10.1029/JA093iA06p05741. URL: https://doi.org/10.1029/JA093iA06p05741.

Russell, C. T., M. Ginskey, and S. M. Petrinec (Jan. 1994). "Sudden impulses at low-latitude stations: Steady state response for northward interplanetary magnetic field". In: *Journal of Geophysical Research: Space Physics* 99.A1, pp. 253–261. DOI: https://doi.org/10.1029/93JA02288.

Sabaka, T. J., G. Hulot, and N. Olsen (2010). "Mathematical Properties Relevant to Geomagnetic Field Modeling". English. In: *Handbook of Geomathematics*. Springer. DOI: 10.1007/978-3-642-27793-1_17-2.

Sabaka, T. J., L. Tøffner-Clausen, N. Olsen, and C. C. Finlay (June 2020). "CM6: a comprehensive geomagnetic field model derived from both CHAMP and Swarm satellite observations". In: *Earth, Planets and Space* 72.1, p. 80. DOI: 10.1186/s40623-020-01210-5. URL: https://doi.org/10.1186/s40623-020-01210-5.

Schaeffer, N., E. Silva, and M. A. Pais (June 2016). "Can Core Flows inferred from Geomagnetic Field Models explain the Earth's Dynamo?" In: *Geophysical Journal International* 204. DOI: 10.6084/m9.figshare.1439333.

Shi, Xueling et al. (2022). "Geospace Concussion: Global Reversal of Ionospheric Vertical Plasma Drift in Response to a Sudden Commencement". In: *Geophysical Research Letters* 49.19. e2022GL100014 2022GL100014, e2022GL100014. DOI: https://doi.org/10.1029/2022GL100014. eprint: https://agupubs.onlinelibrary.wiley.com/doi/pdf/10.1029/2022GL100014. URL: https://agupubs.onlinelibrary.wiley.com/doi/abs/10.1029/2022GL100014.

Slinker, S. P., J. A. Fedder, W. J. Hughes, and J. G. Lyon (1999). "Response of the ionosphere to a density pulse in the solar wind: Simulation of traveling convection vortices". In: *Geophysical Research Letters* 26.23, pp. 3549–3552. DOI: https://doi.org/10.1029/1999GL010688.

Southwood, D. J. and M. G. Kivelson (1991). "An approximate description of field-aligned currents in a planetary magnetic field". In: *Journal of Geophysical Research: Space Physics* 96.A1, pp. 67–75. DOI: https://doi.org/10.1029/90JA01806. eprint: https://agupubs.onlinelibrary.wiley.com/doi/pdf/10.1029/90JA01806.

URL: https://agupubs.onlinelibrary.wiley.com/doi/abs/10.1029/90JA01806.

Strangeway, R. J. (2012). "The equivalence of Joule dissipation and frictional heating in the collisional ionosphere". In: *Journal of Geophysical Research: Space Physics* 117.A2. DOI: https://doi.org/10.1029/2011JA017302. eprint: https://agupubs.onlinelibrary.wiley.com/doi/pdf/10.1029/2011JA017302. URL: https://agupubs.onlinelibrary.wiley.com/doi/abs/10.1029/2011JA017302.

Takeda, Masahiko (2008). "Effects of the induction electric field on ionospheric current systems driven by field-aligned currents of magnetospheric origin". In: *Journal of Geophysical Research: Space Physics* 113.A1. DOI: https://doi.org/10.1029/2007JA012662. eprint: https://agupubs.onlinelibrary.wiley.com/doi/pdf/10.1029/2007JA012662. URL: https://agupubs.onlinelibrary.wiley.com/doi/abs/10.1029/2007JA012662.

Tanaka, T. (2000). "The state transition model of the substorm onset". In: *Journal of Geophysical Research: Space Physics* 105.A9, pp. 21081–21096. DOI: https://doi.org/10.1029/2000JA900061. eprint: https://agupubs.onlinelibrary.wiley.com/doi/pdf/10.1029/2000JA900061. URL: https://agupubs.onlinelibrary.wiley.com/doi/abs/10.1029/2000JA900061.

Thébault, E. et al. (May 2015). "International Geomagnetic Reference Field: the 12th generation". In: *Earth, Planets and Space* 67.1, p. 79. DOI: 10.1186/s40623-015-0228-9. URL: https://doi.org/10.1186/s40623-015-0228-9.

Vanhamäki, H., O. Amm, and A. Viljanen (2006). "New method for solving inductive electric fields in the non-uniformly conducting ionosphere". In: *Annales Geophysicae* 24.10, pp. 2573–2582. DOI: 10.5194/angeo-24-2573-2006. URL: https://angeo.copernicus.org/articles/24/2573/2006/.

— (2007). "Role of inductive electric fields and currents in dynamical ionospheric situations". In: *Annales Geophysicae* 25.2, pp. 437–455. DOI: 10.5194/angeo-25-437-2007. URL: https://angeo.copernicus.org/articles/25/437/2007/.

Vanhamäki, H., A. Viljanen, and O. Amm (2005). "Induction effects on ionospheric electric and magnetic fields". In: *Annales Geophysicae* 23.5, pp. 1735–1746. DOI: 10.5194/angeo-23-1735-2005. URL: https://angeo.copernicus.org/articles/23/1735/2005/.

Vanhamäki, H., A. Viljanen, R. Pirjola, and O. Amm (Sept. 2013). "Deriving the geomagnetically induced electric field at the Earth's surface from the time derivative of the vertical magnetic field". In: *Earth, Planets and Space* 65.9, pp. 997–1006. DOI: 10.5047/eps.2013.03.013. URL: https://doi.org/10.5047/eps.2013.03.013.

Vasyliūnas, V M (Feb. 2012). "The physical basis of ionospheric electrodynamics". In: *Ann. Geophys.* 30.2, pp. 357–369. DOI: 10.5194/angeo-30-357-2012. URL: https://www.ann-geophys.net/30/357/2012/%20https://www.ann-geophys.net/30/357/2012/angeo-30-357-2012.pdf.

Yoshikawa, A. and M. Itonaga (2000). "The nature of reflection and mode conversion of MHD waves in the inductive ionosphere: Multistep mode conversion between divergent and rotational electric fields". In: *Journal of Geophysical Research: Space Physics* 105.A5, pp. 10565–10584. DOI: https://doi.org/10.1029/1999JA000159. eprint: https://agupubs.onlinelibrary.wiley.com/doi/pdf/10.1029/

1999JA000159. URL: https://agupubs.onlinelibrary.wiley.com/doi/abs/10.1029/1999JA000159.

Zou, S., D. Ozturk, R. Varney, and A. Reimer (2017). "Effects of sudden commencement on the ionosphere: PFISR observations and global MHD simulation". In: *Geophysical Research Letters* 44.7, pp. 3047–3058. DOI: https://doi.org/10.1002/2017GL072678. eprint: https://agupubs.onlinelibrary.wiley.com/doi/pdf/10.1002/2017GL072678. URL: https://agupubs.onlinelibrary.wiley.com/doi/abs/10.1002/2017GL072678.

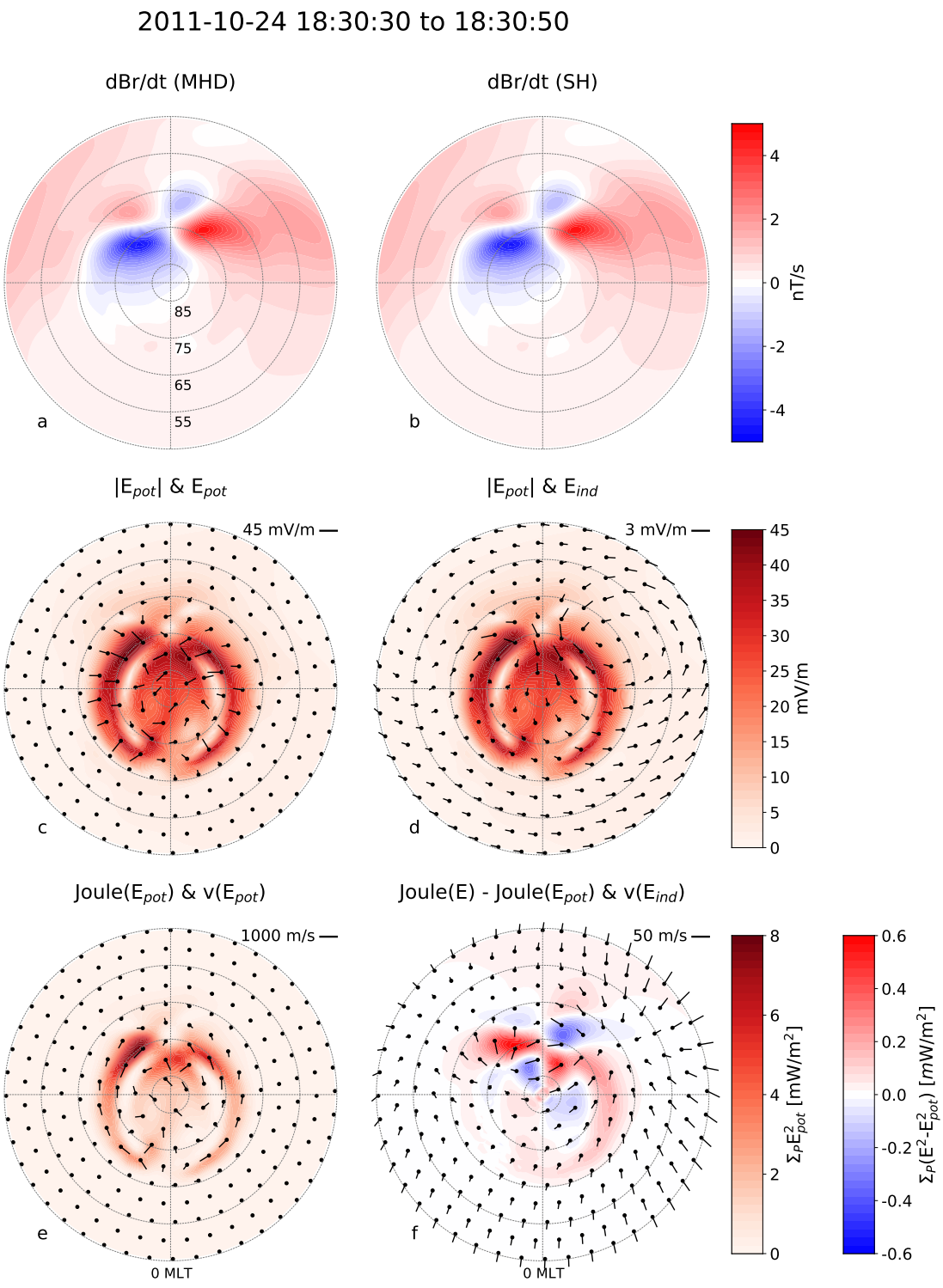

Figure 1. A summary of how $\boldsymbol{E}_{ind}$ is determined based on synthetic ground magnetometer measurements from an MHD simulation [Shi et al. 2022], along with the compression flow and Joule heating. Figures 1a-b show $\frac{\partial}{\partial t}B_r$ from the MHD and SH model, respectively. Figure 1c shows the magnitude of $\boldsymbol{E}_{pot}$ and its orientation as pins. Figure 1d shows the magnitude of $\boldsymbol{E}_{pot}$ with the orientation of $\boldsymbol{E}_{ind}$ overlain. Figure 1e shows the Joule heating and plasma convection associated with $\boldsymbol{E}_{pot}$ as a contour and pins, respectively. Figure 1f shows the difference between Joule heating associated with $\boldsymbol{E}_{pot}$ and $\boldsymbol{E} = \boldsymbol{E}_{pot} + \boldsymbol{E}_{ind}$ as well as the compression flow associated with $\boldsymbol{E}_{ind}$. The purpose of this figure is to validate the SH models' recreation of $\frac{\partial}{\partial t}B_r$ as well as demonstrate the technique for estimating $\boldsymbol{E}_{ind}$.

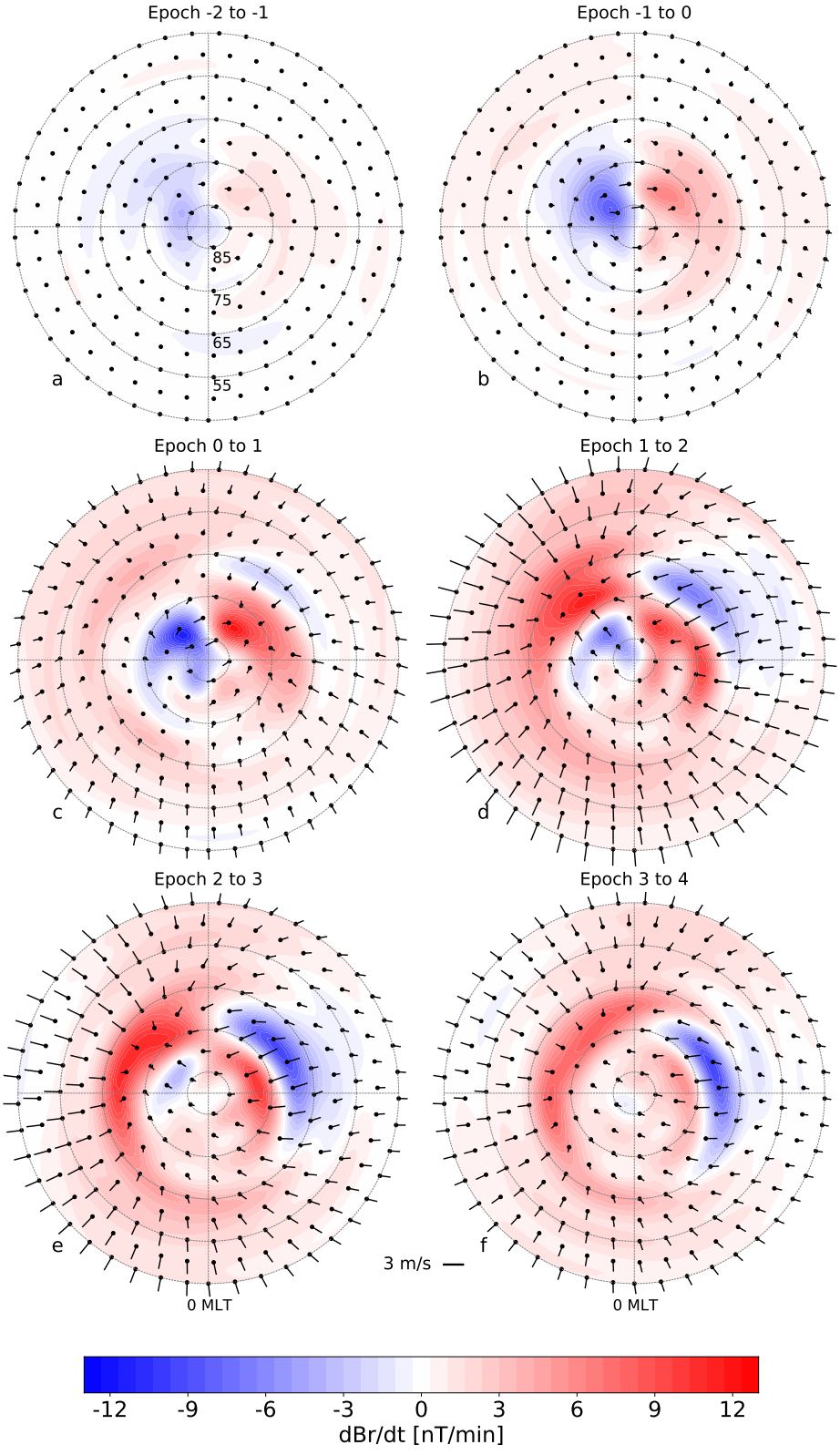

Figure 2. Illustration of $\frac{\partial}{\partial t}B$ and $\boldsymbol{E}_{ind}\times\boldsymbol{B}_0$ drift based on the SH model provided by Madelaire et al. 2022b. Epoch is synonymous with minute. The purpose of this figure is to showcase the estimation of $\boldsymbol{E}_{ind}$ using a SH model that is based on real ground magnetometer measurements. Furthermore, the data includes contributions from magnetospheric sources that give rise to a large-scale southward compression flow.

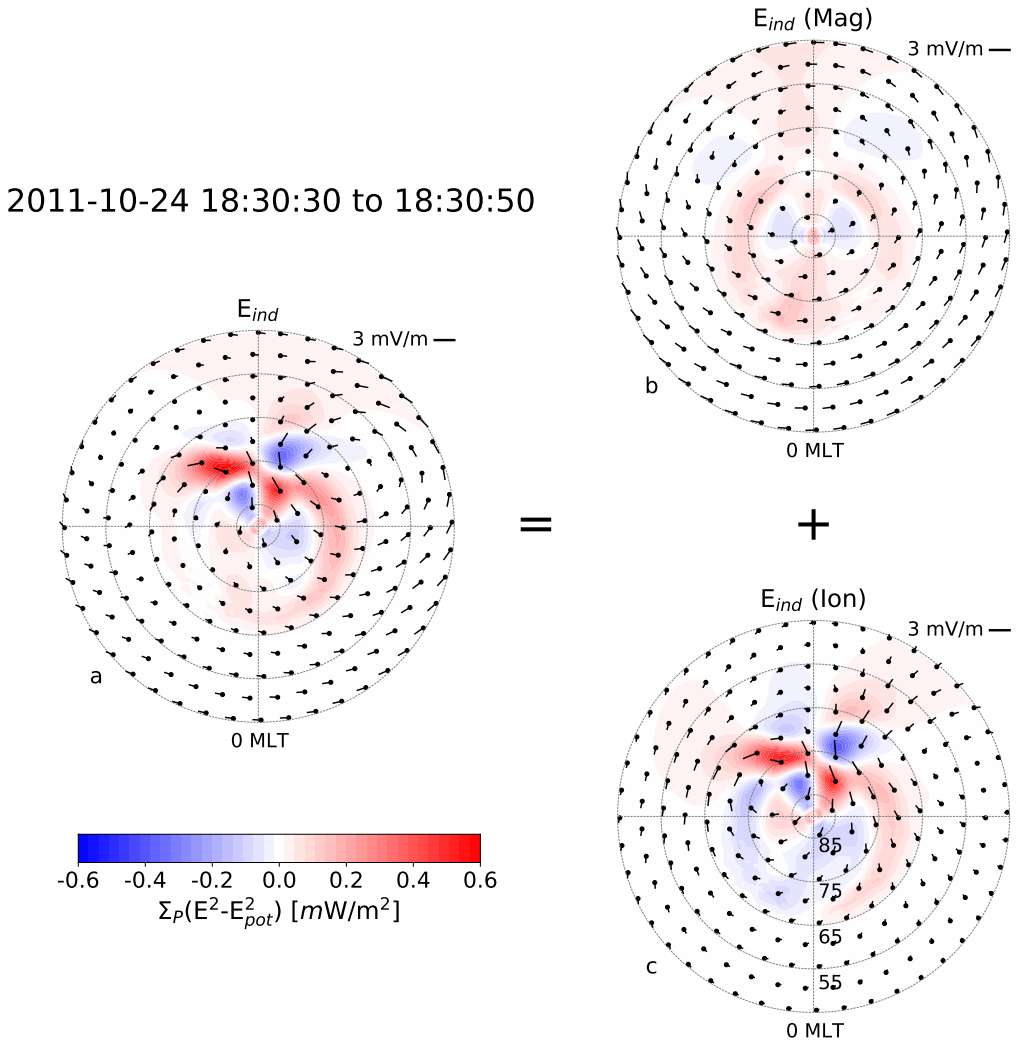

Figure 3. A decomposition of the contribution to $\boldsymbol{E}_{ind}$ and associated Joule heating. Figure 3a shows the modification to the Joule heating when including $\boldsymbol{E}_{ind}$ as a contour similar to Figure 1f with $\boldsymbol{E}_{ind}$ superposed as pins. Figure 3b shows the contribution from magnetospheric currents while Figure 3c shows the contribution from ionospheric currents and FACs.